Theoret. Appl. Mech., Vol.39, No.1, pp. 1–25, Belgrade 2012

A low/high frequency combined approach for the identification of mechanical properties of composite structural elements

Ivan Bartoli* **Alessandro Marzani†**

Abstract

A combined low/high frequency dynamic identification approach is presented. The proposed hybrid technique compares experimentally extracted dynamic properties of plates such as modal frequencies and guided wave dispersion properties with the correspondent numerically predicted ones. Identification of mechanical properties of the plates is achieved by iteratively adjusting the mechanical properties assumed in finite element and semi-analytical models through minimization of the difference between experimental and predicted dynamic features.

Keywords: Dynamic identification, composite plates.

1 Introduction

Composite materials have been widely used in the mechanical and aerospace industry and their use is becoming extremely diffused in civil engineering applications as well. The quality and mechanical properties of composite materials are highly dependent upon the production process. There are many methods for manufacturing laminated composite components and different

*Department of Civil, Architectural and Environmental Engineering, Drexel University, 3141 Chestnut Street, Curtis Hall 251, Philadelphia, PA - USA,e-mail: ibartoli@drexel.edu

†DICAM Department, Faculty of Engineering, ALMA MATER STUDIORUM - University of Bologna, Viale del Risorgimento 2, 40136 Bologna - Italy, e-mail: alessandro.marzani@unibo.it

manufacturing or curing processes can result in variations of mechanical properties. Furthermore, even the most advanced manufacturing system is not capable of producing different parts with perfectly constant and homogeneous properties. Obviously, knowledge of composite material properties is indispensable in the design of structural components. Therefore, in order to monitor the quality of the components at the end of any manufacturing process, techniques capable of estimating their mechanical properties are needed.

Unfortunately the characterization of mechanical properties of fiber reinforced composites presents more difficulties than the characterization of traditional isotropic materials. The identification of the stiffness properties is hampered by the anisotropy of the materials. Conventional static methods for determining mechanical properties show several challenges. For example determining Young's moduli along different principle axes of symmetry of orthotropic materials by classical mechanical approaches requires multiple uniaxial tests. Unfortunately, these techniques are in general destructive approaches because they require cutting specimens to perform the tests in the desired configuration and the determined properties are local as they are representative of the specimen only and not necessarily coincide with the global mechanical properties of the system. However global properties are typically required in order to predict the global response of the structures obtained assembling composite components.

These issues have motivated an increasing attention to global dynamic identification approaches [1, 2, 3, 4]. Many composite components are in the form of plates. These structures, of relatively simple geometry, can be easily tested by non destructive vibration based tests. By modal analysis, the vibration properties of these components (natural frequencies) can be extracted and compared to the associated predicted quantities obtained by updating the stiffness properties of accurate numerical models. The estimated properties that minimize the difference between the numerical model vibration properties and the correspondent experimental parameters can be assumed as the global stiffness elastic constants. While the technique allows the simultaneous identification of the majority of elastic constants/stiffness parameters, constants that scarcely influence the natural frequencies such as Poisson ratio and out of plane Shear constants are difficult to predict. The difficulty of the problem increases when the number of layers in a composite plate is large and the lay-up is complex leading to multiple solutions of the

identification approach.

Different researchers have attempted to improve the identification procedure using different estimators based on Least Square method [3], Bayesian approach [5, 6, 7, 8] or Genetic algorithms [9] as well as employing refined finite element models with high order deformation theory for thick plates to account for out of plane deformation [8]. However, the small sensitivity of the natural frequencies to transverse shear constants and Poisson's ratio remains the major challenge.

In this paper, the authors show how higher frequency vibrations (guided waves) can bridge this gap in the identification approach. Guided waves are potentially sensitive to all the mechanical constants. In particular, flexural modes are affected by out of plane constants. A simple modification of the test set-up and the use of higher frequency vibrations will be discussed to account for guided waves. In the first part of the paper, the authors discuss the identification procedure based on standard low frequency dynamic approach. In the second part, modeling of guided waves and use of their dispersion properties for parameter identification is shown.

2 Low Frequency dynamic identification

In this section a combined numerical-experimental method for the identification of the mechanical properties of thick composite plates made of different materials and with general stacking sequence is described. The approach described is an extension of the work by Lai and Ip [5]. The identification technique is performed by the comparison of experimental data with the results produced by numerical methods.

Modeling: The numerical model used is based on a first order shear deformation theory [10] used in a finite element model and allows the prediction of the dynamic behavior of the system. Fig.1 shows a rectangular composite plate with N orthotropic layers. A Cartesian coordinate system (x,y,z) is located in the middle plane. h, $a$and b represent the dimensions in the z-, x- and y- direction, respectively. The k-th orthotropic layer has the fibers rotated of an angle θ^k with respect to the $x$axis. The in-plane displacements u and $v$and the out-of-plane displacement w can be expressed according to

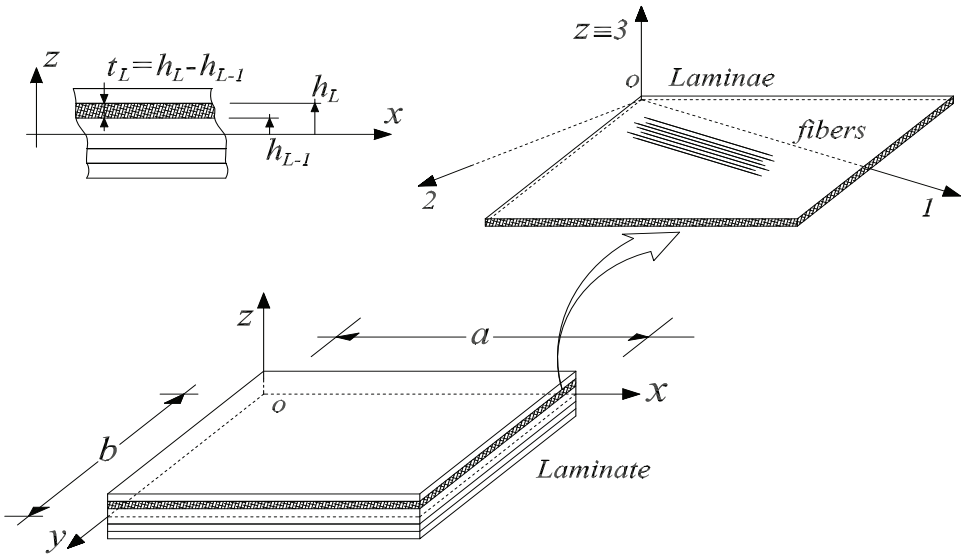

Figure 1: Laminated composite plate.

the first shear deformation theory as follows [10]

$$\begin{aligned} u(x,y,z,t) &= u_0(x,y,t) + z\beta_x(x,y,t) \\ v(x,y,z,t) &= v_0(x,y,t) + z\beta_y(x,y,t) \\ w(x,y,z,t) &= w_0(x,y,t) \end{aligned} \tag{1}$$

where u_0, v_0, w_0 are the mid-plane displacements of the plate and β_x, β_y are the rotations of the normal about the y and x- axes respectively. The strain-displacement relations can be taken as

$$\begin{aligned} \varepsilon_x &= \frac{\partial u_0}{\partial x} + z\frac{\partial \beta_x}{\partial x} = \varepsilon_x^0 + z\chi_x, \qquad \varepsilon_y = \frac{\partial v_0}{\partial y} + z\frac{\partial \beta_y}{\partial y} = \varepsilon_y^0 + z\chi_y \\ \gamma_{xy} &= \frac{\partial u_0}{\partial y} + \frac{\partial v_0}{\partial x} + z\left(\frac{\partial \beta_x}{\partial y} + \frac{\partial \beta_y}{\partial x}\right) = \gamma_{xy}^0 + z\chi_{xy} \\ \gamma_{xz} &= \beta_x + \frac{\partial w_0}{\partial x}, \qquad \gamma_{yz} = \beta_y + \frac{\partial w_0}{\partial y} \end{aligned} \tag{2}$$

For the *k-th* layer of the plate, the principal orthogonal material axes

(1,2,3) are defined and the stress strain relations can be written as [10]

$$\begin{bmatrix} \sigma_1^k \\ \sigma_2^k \\ \tau_{12}^k \\ \tau_{13}^k \\ \tau_{23}^k \end{bmatrix} = \begin{bmatrix} \bar{C}_{11}^k & \bar{C}_{12}^k & 0 & 0 & 0 \\ \bar{C}_{12}^k & \bar{C}_{22}^k & 0 & 0 & 0 \\ 0 & 0 & \bar{C}_{33}^k & 0 & 0 \\ 0 & 0 & 0 & \bar{C}_{44}^k & 0 \\ 0 & 0 & 0 & 0 & \bar{C}_{55}^k \end{bmatrix} \begin{bmatrix} \varepsilon_1^k \\ \varepsilon_2^k \\ \gamma_{12}^k \\ \gamma_{13}^k \\ \gamma_{23}^k \end{bmatrix} \tag{3}$$

where the normal stress σ_3^k is neglected and the transverse shear stresses τ_{13}^k and τ_{23}^k are included. In Eq.(3) σ_1^k, σ_2^k and τ_{12}^k represent the in plane stresses; ε_1^k, ε_2^k, γ_{12}^k, γ_{13}^k and γ_{23}^k are the strain deformation components. The plane stress-reduced stiffnesses

$$\begin{aligned} \bar{C}_{11}^k &= \frac{E_1^k}{1-\nu_{12}^k\nu_{21}^k}, \quad \bar{C}_{22}^k = \frac{E_2^k}{1-\nu_{12}^k\nu_{21}^k}, \\ \bar{C}_{12}^k &= \frac{\nu_{12}^k E_2^k}{1-\nu_{12}^k\nu_{21}^k} = \frac{\nu_{21}^k E_1^k}{1-\nu_{12}^k\nu_{21}^k} \\ \bar{C}_{33}^k &= G_{12}^k, \qquad \bar{C}_{44}^k = G_{13}^k, \qquad \bar{C}_{55}^k = G_{23}^k \end{aligned} \tag{4}$$

are given as functions of the two Young moduli E_1^k, E_2^k, Poisson ratios ν_{12}^k, ν_{21}^k and elastic shear moduli G_{12}^k, G_{13}^k and G_{23}^k. The transformed stress-strain relations with respect to the reference system (x, y, z) can be obtained as

$$\begin{bmatrix} \sigma_x^k \\ \sigma_y^k \\ \tau_{xy}^k \\ \tau_{xz}^k \\ \tau_{yz}^k \end{bmatrix} = \begin{bmatrix} C_{11}^k & C_{12}^k & C_{13}^k & 0 & 0 \\ C_{12}^k & C_{22}^k & C_{23}^k & 0 & 0 \\ C_{13}^k & C_{23}^k & C_{33}^k & 0 & 0 \\ 0 & 0 & 0 & C_{44}^k & C_{45}^k \\ 0 & 0 & 0 & C_{45}^k & C_{55}^k \end{bmatrix} \begin{bmatrix} \varepsilon_x^0 + z\chi_x \\ \varepsilon_y^0 + z\chi_y \\ \gamma_{xy}^0 + z\chi_{xy} \\ \gamma_{xz}^k \\ \gamma_{yz}^k \end{bmatrix} \tag{5}$$

where

$$\begin{aligned} C_{11}^k &= \bar{C}_{11}^k m^4 + 2\left(\bar{C}_{12}^k + 2\bar{C}_{33}^k\right) n^2 m^2 + \bar{C}_{22}^k n^4 \\ C_{12}^k &= \left(\bar{C}_{11}^k + \bar{C}_{22}^k - 4\bar{C}_{33}^k\right) n^2 m^2 + \bar{C}_{12}^k \left(n^4 + m^4\right) \\ C_{22}^k &= \bar{C}_{11}^k n^4 + 2\left(\bar{C}_{12}^k + 2\bar{C}_{33}^k\right) n^2 m^2 + \bar{C}_{22}^k m^4 \\ C_{13}^k &= \left(-\bar{C}_{11}^k + \bar{C}_{12}^k + 2\bar{C}_{33}^k\right) n m^3 + \left(-\bar{C}_{12}^k + \bar{C}_{22}^k - 2\bar{C}_{33}^k\right) n^3 m \\ C_{12}^k &= C_{21}^k, \quad C_{31}^k = C_{13}^k, \quad C_{32}^k = C_{23}^k, \quad C_{45}^k = C_{54}^k \\ C_{33}^k &= \left(\bar{C}_{11}^k + \bar{C}_{22}^k - 2\bar{C}_{12}^k - 2\bar{C}_{33}^k\right) n^2 m^2 + \bar{C}_{33}^k \left(n^4 + m^4\right) \end{aligned} \tag{6a}$$

$$
\begin{aligned}
C_{23}^k &= \left(-\bar{C}_{11}^k + \bar{C}_{12}^k + 2\bar{C}_{33}^k\right) n^3 m + \left(-\bar{C}_{12}^k + \bar{C}_{22}^k - 2\bar{C}_{33}^k\right) n m^3 \\
C_{44}^k &= G_{13}^k m^2 + G_{23}^k n^2, \quad C_{45}^k = \left(G_{23}^k - G_{13}^k\right) nm, \\
C_{55}^k &= G_{13}^k n^2 + G_{23}^k m^2
\end{aligned} \tag{6b}
$$

and $n = \sin\theta^k, \quad m = \cos\theta^k$ [10, 11].

The weak form of the governing equation for the vibration analysis can be obtained by means of the Hamilton's principle. The expressions of the kinetic energy T and potential energy U read as:

$$
\begin{aligned}
T &= \frac{1}{2}\int_S \sum_{k=1}^{n} \int_{h_{k-1}}^{h_k} \rho^k \left[\, \dot{u}^2 + \dot{v}^2 + \dot{w}^2 \right] dz dS = \frac{1}{2} I_1 \int_0^a \int_0^b \left[\dot{u}_0^2 + \dot{v}_0^2 + \dot{w}_0^2\right] dx dy \\
&+ I_2 \int_0^a \int_0^b \left[\dot{u}_0 \dot{\beta}_x + \dot{v}_0 \dot{\beta}_y\right] dx dy + \frac{1}{2} I_3 \int_0^a \int_0^b \left[\dot{\beta}_x^2 + \dot{\beta}_y^2\right] dx dy \\
U &= \frac{1}{2}\int_S \sum_{k=1}^{n} \int_{h_{k-1}}^{h_k} (\sigma_x^k \varepsilon_x^k + \sigma_y^k \varepsilon_y^k + \tau_{xy}^k \gamma_{xy}^k + \tau_{xz}^k \gamma_{xz}^k + \tau_{yz}^k \gamma_{yz}^k\,) dz dS = \\
&= \frac{1}{2}\int_S \left(N_x \varepsilon_x^0 + M_x \chi_x + N_y \varepsilon_y^0 + M_y \chi_y + N_{xy} \gamma_{xy}^0 \right. \\
&\left. + M_{xy}\chi_{xy} + Q_{xz}\gamma_{xz} + Q_{yz}\gamma_{yz}\right) dS
\end{aligned} \tag{7}
$$

In Eq.(25) the stress resultants are defined as:

$$
\begin{bmatrix} N_x \\ N_y \\ N_{xy} \end{bmatrix} = \sum_{k=1}^{n} \int_{h_{k-1}}^{h_k} \begin{bmatrix} \sigma_x^k \\ \sigma_y^k \\ \tau_{xy}^k \end{bmatrix} dz, \quad \begin{bmatrix} M_x \\ M_y \\ M_{xy} \end{bmatrix} = \sum_{k=1}^{n} \int_{h_{k-1}}^{h_k} \begin{bmatrix} \sigma_x^k \\ \sigma_y^k \\ \tau_{xy}^k \end{bmatrix} z dz,
$$

$$
\begin{matrix} Q_x \\ Q_y \end{matrix} = \sum_{k=1}^{n} \int_{h_{k-1}}^{h_k} \begin{bmatrix} \tau_{xz}^k \\ \tau_{yz}^k \end{bmatrix} dz \tag{8}
$$

while

$$
I_1 = \sum_{k=1}^{n} \int_{h_{k-1}}^{h_k} \rho^k dz, \quad I_2 = \sum_{k=1}^{n} \int_{h_{k-1}}^{h_k} \rho^k z dz, \quad I_3 = \sum_{k=1}^{n} \int_{h_{k-1}}^{h_k} \rho^k z^2 dz \tag{9}
$$

are the translational, coupling and rotational moments of inertia. By introducing the stress-strain relations of Eq.(5) in Eq.(7), the potential energy becomes

$$U = \frac{1}{2}\int_S \left[\varepsilon_0^T \mathbf{A}\varepsilon_0 + \chi^T \mathbf{B}\varepsilon_0 \; + \varepsilon_0^T \mathbf{B}\chi + \chi^T \mathbf{D}\chi + \gamma^T \mathbf{H}\gamma\right] dS \tag{10}$$

In the above energy expression

$$\varepsilon_0 = \left[\begin{array}{c} \varepsilon_x^0 \\ \varepsilon_y^0 \\ \gamma_{xy}^0 \end{array}\right] = \left[\begin{array}{c} \dfrac{\partial u_0}{\partial x} \\ \dfrac{\partial v_0}{\partial y} \\ \dfrac{\partial u_0}{\partial y} + \dfrac{\partial v_0}{\partial x} \end{array}\right], \chi = \left[\begin{array}{c} \chi_x \\ \chi_y \\ \chi_{xy} \end{array}\right] = \left[\begin{array}{c} \dfrac{\partial \beta_x}{\partial x} \\ \dfrac{\partial \beta_y}{\partial y} \\ \dfrac{\partial \beta_x}{\partial y} + \dfrac{\partial \beta_y}{\partial x} \end{array}\right],$$

$$\gamma = \left[\begin{array}{c} \gamma_{xz} \\ \gamma_{yz} \end{array}\right] = \left[\begin{array}{c} \beta_x + \dfrac{\partial w_0}{\partial x} \\ \beta_y + \dfrac{\partial w_0}{\partial y} \end{array}\right] \tag{11}$$

and $\mathbf{A}_{3\times3}$, $\mathbf{B}_{3\times3}$, $\mathbf{D}_{3\times3}$, $\mathbf{H}_{2\times2}$, are matrices with elements defined as

$$\begin{aligned} (A_{ij}, B_{ij}, D_{ij}) &= \sum_{k=1}^{n} \int_{h_{k-1}}^{h_k} C_{ij}^k \left(1, z, z^2\right) dz, \quad (i,j = 1,2,3)\,; \\ H_{ij} &= \kappa^2 \sum_{k=1}^{n} \int_{h_{k-1}}^{h_k} C_{ij}^k dz \, (i,j = 4,5) \end{aligned} \tag{12}$$

with κ^2 representing the shear correction factor that is assumed to be 5/6. In the present study a rectangular element with 16 nodes is implemented. More details on the element used and on the shape functions can be found elsewhere [12]. For each element, the displacement functions are interpolated as

$$\begin{aligned} u_0 &= \mathbf{N}^T \mathbf{u}_0, \quad v_0 = \mathbf{N}^T \mathbf{v}_0, \quad w_0 = \mathbf{N}^T \mathbf{w}_0, \\ \beta_x &= \mathbf{N}^T \beta_x, \quad \beta_y = \mathbf{N}^T \beta_y \end{aligned} \tag{13}$$

where $\mathbf{N}^T$ is a 16×1 shape function matrix while $\mathbf{u}_0$, $\mathbf{v}_0$,$\mathbf{w}_0$,β_x and β_y are the 16×1 vectors containing the nodal generalized displacements. The plate domain can be subdivided into $m \times n$ finite elements and after standard finite element assembling procedures are used, the equation governing the free harmonic motion of the plate system considered is obtained as:

$$\left(\mathbf{K} + \omega^2 \mathbf{M}\right) \mathbf{V} = \mathbf{0} \tag{14}$$

where $\mathbf{K}$ and $\mathbf{M}$ correspond to the global stiffness matrix and the global mass matrix, and $\mathbf{V}$ is the global nodal displacement amplitude vector for a harmonic motion at frequency ωs defined as $\mathbf{v} = \mathbf{V}\ \exp(i\omega t)$.

When geometry and mechanical properties are known, Eq.(14) represents an eigenvalue problem that allows us to evaluate the eigenfrequencies ω and the associated eigenvectors $\mathbf{V}$ of the plate. In order to model the experimental set up generally employed, the plate will be considered to have free edges. In fact, an accurate determination of the experimental frequencies is usually obtained by suspending the plate with elastic wires in a vertical position that closely approximates a free boundary condition. Therefore the solution of the eigenvalue problem leads also to six null eigenvalues, associated to eigenvectors (modeshapes) with zero potential energy, representing the six rigid body modes: the three rigid translations in the x, y and z directions and three rigid rotations around the same coordinate axis.

Estimation Procedure: In this section, the method of Bayesian estimation discussed by Lai and Ip [5] for the determination of the elastic constants of generally thin orthotropic plates is extended to the case of thick plates with a general sequence of layers. The present Bayesian approach implies the minimization of the error function

$$e(\mathbf{r}, \mathbf{p}) = (\widehat{\mathbf{r}} - \mathbf{r})^T \mathbf{C}_R (\widehat{\mathbf{r}} - \mathbf{r}) + (\mathbf{p} - \mathbf{p}_0)^T \mathbf{C}_P (\mathbf{p} - \mathbf{p}_0) \tag{15}$$

where

$$\widehat{\mathbf{r}} = \left[\lambda_{\exp 1} \lambda_{\exp 2} ... \lambda_{\exp N}\right]^T, \quad \mathbf{r} = \left[\lambda_1 \lambda_2 ... \lambda_N\right]^T, \tag{16}$$

are the vectors of measured and numerically predicted eigenvalues/frequencies, and

$$\begin{aligned} \mathbf{p} &= \left[\bar{C}_{11} \bar{C}_{12} \bar{C}_{22} \bar{C}_{33} \bar{C}_{44} \bar{C}_{55}\right]^T, \\ \mathbf{p}_0 &= \left[\bar{C}_{11,0} \bar{C}_{12,0} \bar{C}_{22,0} \bar{C}_{33,0} \bar{C}_{44,0} \bar{C}_{55,0}\right]^T \end{aligned} \tag{17}$$

represent the vectors of updated and initial parameters.

The coefficients in eq.(16) can be evaluated as follows

$$\lambda_i = \rho h \omega_i^2 a^2 b^2 \tag{18}$$

The identification method finds the minimum of the error function $e(\mathbf{r},\mathbf{p})$. Each parameter has a weight assigned through diagonal matrices written as:

$$\begin{aligned} \mathbf{C}_R &= diag\left(\frac{1}{\delta^2(\lambda_{\exp 1})},\ \frac{1}{\delta^2(\lambda_{\exp 2})},\ ...,\ \frac{1}{\delta^2(\lambda_{\exp_N})}\right), \\ \mathbf{C}_P &= diag\left(\frac{1}{\delta^2(p_{1,0})},\ \frac{1}{\delta^2(p_{2,0})},\ ...,\ \frac{1}{\delta^2(p_{6,0})}\right) \end{aligned} \tag{19}$$

The choice of the above quantities influences the iterative identification procedure. $\mathbf{C}_R$ and $\mathbf{C}_P$ represent the confidence in the frequencies and in the initial values of the mechanical properties. The elements of these matrices can be evaluated as discussed in [5]. More details on the Bayesian approach can also be found in [6]. For the sake of brevity, the final expression used in the updating process is here shown

$$\mathbf{p} = \mathbf{p}_0 + \left(\mathbf{C}_P + \mathbf{S}|_{\tilde{\mathbf{p}}}^T\ \mathbf{C}_R\ \ \mathbf{S}|_{\tilde{\mathbf{p}}}\right)^{-1} \mathbf{S}|_{\tilde{\mathbf{p}}}^T\ \ \mathbf{C}_R \left(\widehat{\mathbf{r}} - \tilde{\mathbf{r}} - \mathbf{S}|_{\tilde{\mathbf{p}}}\left(\mathbf{p}_0 - \tilde{\mathbf{p}}\right)\right) \tag{20}$$

where $\mathbf{S}|_{\tilde{\mathbf{p}}}$ is the sensitivity stiffness matrix computed as in [6].

Results: The identification results obtained for a woven composite plate are here shown. More results are presented in [13]. The test plate was suspended as in Fig.2(a) with thin wires in order to accurately approximate the free-free boundary conditions assumed in the FEM model. The plate was excited by an impulse impact hammer (PCB 086D80 mini hammer) and the vibrations measured with 4 accelerometers. These 4 accelerometers where used to guarantee an accurate determination of the frequencies of the plate avoiding the risk that one of them would be positioned on a nodal line. Since the excitation force was not recorded in the tests the "peak picking" approach was used to identify the resonance frequencies from the position of the respective peaks in the frequency spectrum. A typical signal recorded is shown in Fig. 2(b) and the Fast Fourier Transform is represented in Fig. 2(c). By observing the FFT plots of signals #1 and #2 overlapped in Fig. 2(c), it can be noted that some peaks cannot be easily identified by looking only at the FFT of one accelerometer signal. This is generally due to the position

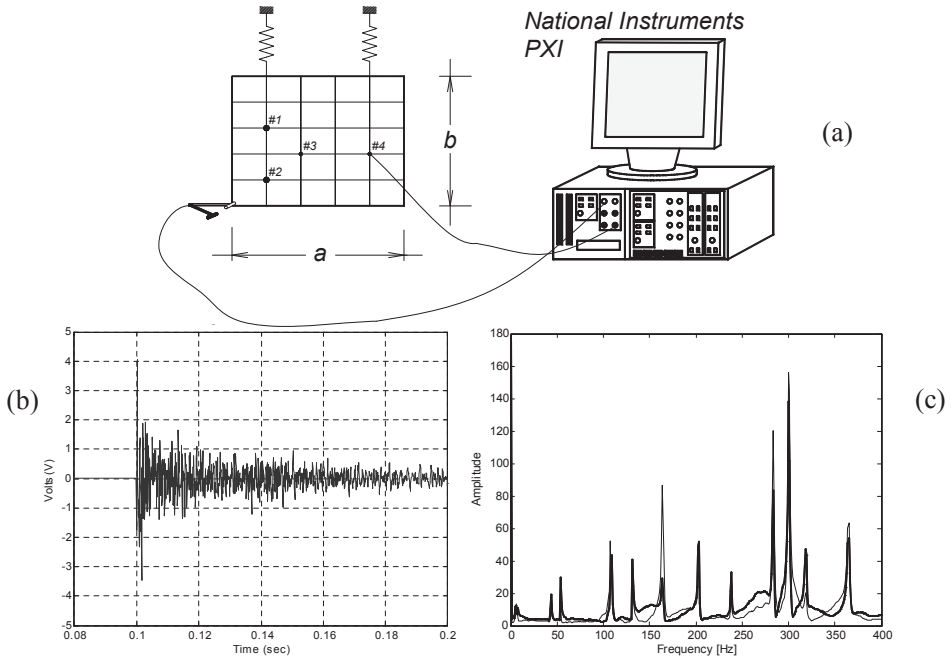

Figure 2: Experimental setup: (a) suspended plate and acquisition system; (b) Typical acceleration time history recorded from vibration of a plate specimen; (c) Fast Fourier Transform computed on acceleration time history.

of the sensors that might be close to the nodal lines of the specific mode considered. The experimental frequencies estimated for the woven plate are collected in Table 1. In the FEM model for frequencies prediction the layers of the composite plate are all assumed to have uniform thickness and same elastic constants. The results for 100 identifications, considering each time a different initial guess for the initial parameters, are shown in Fig. 3. All the simulations shown were successful, i.e. the maximum difference between the experimental frequencies and the numerical frequencies, computed with the estimated values of the parameters, were less than 2%. While for the Young modules and the in plane shear modulus a very low dispersion of the identified values was observed, the Poisson's ratio and the transverse shear modules shown a completely different behavior. In fact these quantities have final values that are highly sparse and a change of the initial values of these parameters produce large changes of their final estimates. This phenomenon

Table 1: Experimental frequencies for a woven composite plate.

	1	2	3	4	5	6	7	8
Freq.[Hz]	37.3	85.8	110.9	211.6	222.3	235.6	257.1	268.2

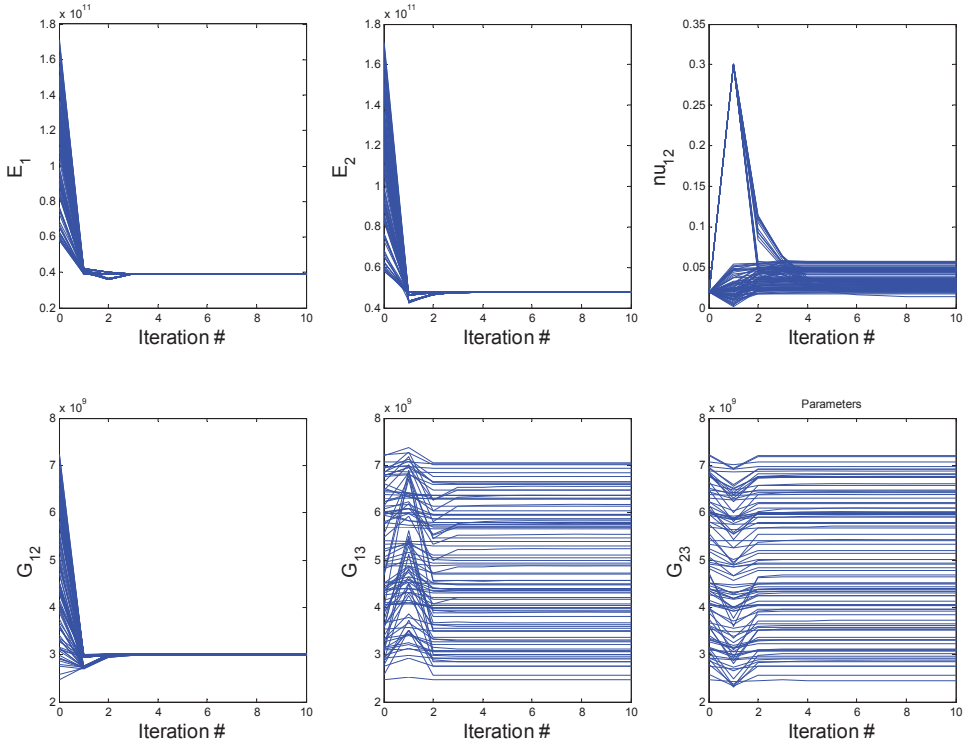

Figure 3: Results of the iterative identification procedure for a composite woven plate.

is expected. It is well known in fact that the Poisson's ratio does not influence the flexural vibrations of the plate. Transversal shear constants, instead, can generally affect the dynamic behavior of thick plates while thin plates show a relatively small shear deformation and the deformation is mainly induced by bending. That also explains why the description of the flexural behavior of thin plates can be done using the classical plate deformation theory [10]. As well known, in this theory the effect of shear deformation is neglected and

the constants G_{13} and G_{23} are not even considered.

Frequently, the proposed procedure will poorly estimate out of plane shear elastic constants as well as Poisson's ratio due to the small influence that these parameters have on the flexural vibration of the plate. Many of the specimens of interest in practice are relatively thin therefore natural modes are not affected by shear deformation in the low frequency range. As a result, the only possibility to have an accurate measure of the out of plane shear constants (G_{13} and G_{23}), is to cut the plate, increasing the thickness-length ratio. Naturally this approach will be a destructive method because the specimen will be destroyed.

As an alternative, the use of higher frequency guided waves is herein considered. For example, asymmetric modes are highly influenced by the transverse shear constants and can be an ideal tool to identify these modules.

3 High Frequency dynamic identification

Resonant frequencies previously discussed refer to the stationary global vibration of the plate. Experimentally, time histories with duration of seconds are necessary to capture these low frequency vibrations. If time histories considered are sampled using higher sampling rates, it is possible to "zoom in" the initial part of the time history and extract the transient vibration of the structure. Transient vibration is governed by the propagation of guided stress waves that are high frequency waves propagating along the plate that behaves as a waveguide. Guided waves can be modeled using traditional finite element method. However, due to the high frequency/small wavelength, a large number of elements is necessary (typical element size is 1/10-1/20 of the smallest wavelength of interest). An approach that has been used to overcome this difficulty is often referred to as semi-analytical finite element (SAFE) method and is extensively presented for example in [14] and [15].

Modeling Guided Waves: The SAFE technique allows to predict the transient propagation of guided waves (time history response) and to extract their properties. A major property of guided waves is the dispersive behavior (their speed changes with the frequency) that results in the time spreading of a short duration pulse when the waves propagate for long distances. The SAFE method accounts for the transient harmonic motion that is typical of a propagating wave at a defined frequency and imposes harmonic motion along the direction of propagation of the wave (x). This is accomplished impos-

ing the exponential harmonic function $e^{i(kx-\omega t)}$ for a mode with frequency ω=$2\pi f$ and wavenumber k=$2\pi/\lambda$g(gλg=wavelengthpugs a result, the approach requires only the discretization along the plate thickness where the displacement is interpolated according to the finite element approach. The displacement field is consequently approximated as [15]:

$$\mathbf{u}^{(e)}(x,y,z,t) = \mathbf{N}(z)\mathbf{q}^{(e)}e^{i(kx-\omega t)} \tag{21}$$

where for the finite element (e) along the thickness, the displacement vector $\mathbf{u}^{(e)}$ depends on the shape function matrix $\mathbf{N}^{(e)}$ and the nodal displacement vector $\mathbf{q}^{(e)}$. Under the displacement assumption of Eq.(21), the equations of motion lead to the following system of equations [14]:

$$(\mathbf{A} - k\mathbf{B})\,\mathbf{Q} = \mathbf{p} \tag{22}$$

where $\mathbf{A}$ and $\mathbf{B}$ are matrices that depend on the stiffness and mass of the plate, $\mathbf{Q}$ is the displacement vector and $\mathbf{p}$ accounts for the loading terms.

Once the eigenvalue problem ($\mathbf{A}$-$k\mathbf{B}$)$\mathbf{Q}$=$\mathbf{0}$ extracted from Eq.(22) is solved for each frequency in the range of interest, and information on propagating modes are stored (wavenumbers and modeshapes of all M propagating modes) the SAFE can be used to a) obtain the dispersion properties such as group velocity vs frequency and b) to compute the response due to a generic stationary or transient excitation. The forced solution for a load applied at $x = x_S$ is computed at each frequency as a combination of all the propagating modes using the equation [14]

$$\mathbf{U}\,(x,\omega) = \sum_{m=1}^{2M} -\frac{\Phi_m^L \tilde{\mathbf{p}}}{B_m}\Phi_m^{Rup}e^{i[k_m(x-x_S)]} \tag{23}$$

where Φ_m^L is the left eigenvector computed from the eigenvalue problem, Φ_m^{Rup} is the half upper-part of the right eigenvector Φ_m^R, $\tilde{\mathbf{p}}$ contains the amplitudes of the nodal loads and $B_m = \Phi_m^L\mathbf{B}\Phi_m^R$. When a hammer excitation is provided to the plate, the force is perpendicular to the plate (z direction). Consequently, the concentrated load assumed in the SAFE can be applied in a point $x = x_S$and assumed acting along the z direction.

Eq.(23) represents the response to a pure harmonic excitation with temporal frequency f and unitary amplitude. The response to an excitation with arbitrary time history (such as an hammer excitation) can be computed as

well. First the frequency content $F(\omega)$ of the excitation signal $F(t)$ must be evaluated by applying the Fourier transform:

$$F(\omega) = \int_{-\infty}^{\infty} F(t) e^{-i2\pi ft} dt \tag{24}$$

The response in the frequency domain to the above force can be computed as:

$$\mathbf{V}(x,\omega) = F(\omega) \cdot \mathbf{U}(x,\omega) = F(\omega) \cdot \sum_{m=1}^{M} -\frac{\Phi_m^L \tilde{\mathbf{P}}}{B_m} \Phi_m^{Rup} e^{i[k_m(x-x_S)]} \tag{25}$$

Finally, the time-domain response can be obtained using the inverse Fourier Transform,

$$\mathbf{V}(x,t) = \frac{1}{2\pi} \int_{-\infty}^{\infty} \mathbf{V}(x,\omega) e^{i2\pi ft} d\omega \tag{26}$$

Once the displacement field is known, the response R_{SAFE} of a sensor (such as a strain gage or a piezoelectric sensor) can be estimated. For a strain gage, the response can be provided by the average strain in the region where the sensor is bonded. In the case an accelerometer is employed, the displacement time history can be derived twice with respect to time to predict an acceleration time history. For example, Fig. 4(b) shows the strain time history predicted using the SAFE analysis. The case modeled is that of a 3.175 mm aluminum plate, subjected to an impact force time history shown in the Fig. 4(a). The sensor is located at a distance of 0.375 m from the source.

The SAFE method can be used as part of an identification algorithm that uses guided wave (high frequency) properties instead of (low frequency) global vibration properties. Prediction of mechanical parameters can be attempted by using group velocities (speed vs frequency) of guided ultrasonic waves. Group velocities must be estimated experimentally.

Continuous Wavelet Transform for guided wave group velocity measure: Based on the signal recorded in a single location as the one predicted by SAFE and illustrated in Fig. 4(b), a joint time frequency transform can be used to extract experimental dispersion group velocities. The method shown is based on the Continuous Wavelet Transform (CWT). The CWT is

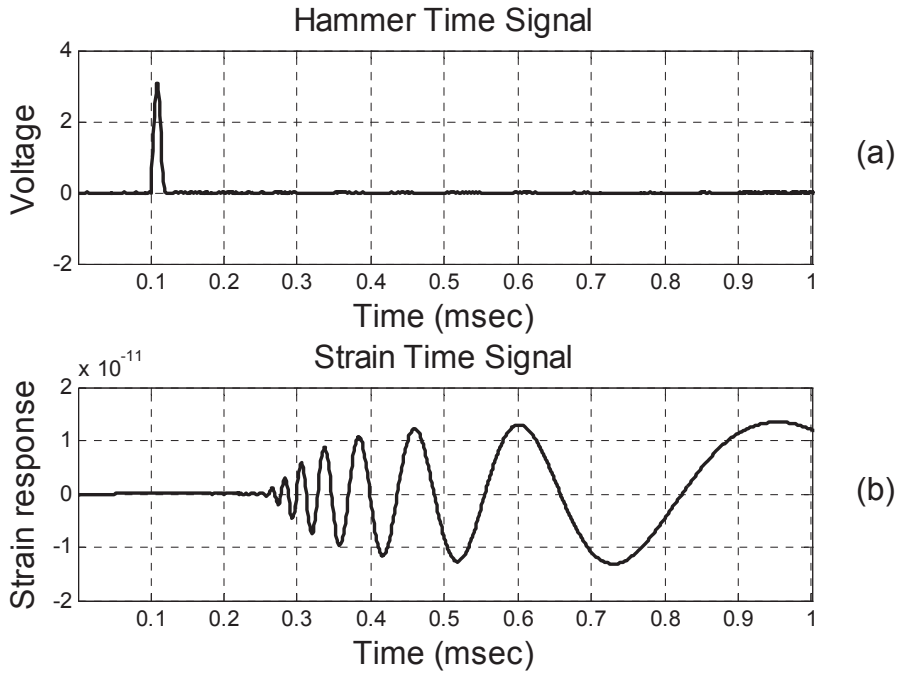

Figure 4: Transient response predicted using the SAFE method in a 3.175 mm aluminum plate: (a) hammer excitation time history; (b) strain time history for a gage at 0.375m from the source.

an approach alternative to the Short Time Fourier Transform. The latter, while providing the joint time-frequency analysis of a time history does not have a multi-resolution capability because a constant time window is used. The CWT uses a flexible window that is broader in time for observing low frequencies and shorter in time for observing high frequencies (Kishimoto et al. 1995).

The wavelet transform decomposes the original signal by computing its correlation with a short-duration wave, the mother wavelet that is flexible in time and in frequency. The CWT of a function $f(t)$ is defined as [17] :

$$Wf(u,s) = \int_{-\infty}^{\infty} f(t) \cdot \frac{1}{\sqrt{s}} \cdot \psi^* \left(\frac{t-u}{s} \right) \cdot dt \tag{27}$$

where ψ^* is the complex conjugate of a function, the mother wavelet $\psi(t)$,

with:

$$\psi_{u,s}(t) = \frac{1}{\sqrt{s}} \cdot \psi \left(\frac{t-u}{s} \right) \tag{28}$$

The mother wavelet can be viewed as a windowing function in time and in frequency domains where u is called the translation parameter, and s is the scaling parameter. The parameter u shifts the wavelet in time and s controls the wavelet frequency bandwidth, hence the time-frequency resolution of the analysis. The scalogram represents the magnitude of the wavelet transformed signal, i.e. the energy density spectrum and it shows the signal energy with different frequencies ωg=gηvs (η being the wavelet center frequency) at various times $t = u$. The scalogram may be displayed in 3-D plots of time-frequency-amplitude. Because the scalogram provides the time–frequency information of the energy components of a function, it is possible to extract the dispersion curves in term of the group velocity. An example of a CWT scalogram is given in Fig. 5 that shows the joint time-frequency transform of the hammer time history previously shown in Fig 4(a) and the CWT transform of the strain waveform predicted by SAFE and illustrated in Fig. 4(b). The guided wave is an anti-symmetric Ao mode excited by the imposed anti-symmetric force applied on the aluminum plate. In the specific case a Complex Morlet Wavelet (center frequency equal to 1, bandwidth parameter equal to 2) was used to extract the Scalograms in Fig. 5. In the CWT scalograms, amplitudes are plotted versus frequency (y-axis) and time (x-axis).

At each frequency, a section of the Scalograms was performed to estimate the arrival time of the wave as a function of the frequency. The sections of the two separate Scalograms are shown in Fig.6 for both the hammer and strain time histories. The time corresponding to the Scalogram peaks are shown in Fig. 5(c) and 5(d). It is observed that while the hammer excitation provides a broadband signal (large frequency range) where all the frequencies are exited simultaneously, the guided mode Ao has different time of arrival at different frequencies. This dispersive behavior is characteristic of guided waves. It follows that the speed for the Ao mode increases for higher frequencies. The group velocity $C_g(f)$ of the mode can be estimated dividing the distance between the hammer point of impact and the sensor ($d = 0.375m$) by the time delays ($t_2(f)t_1(f)$) measured at each frequency and estimated in Fig.5(c) and 5(d). The group velocity obtained can be compared to the numerical group velocity $C_g^{SAFE}(f)$ calculated numerically using the semi analytical finite element method previously represented.

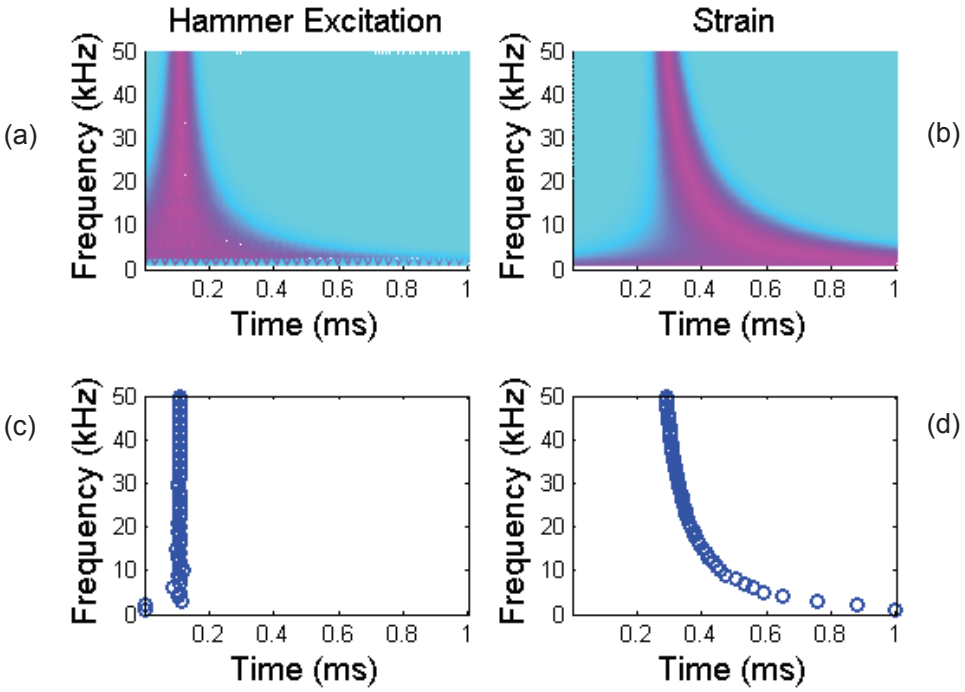

Figure 5: Complex Morlet wavelet scalogram of the hammer (a) and strain (b) waveforms shown in Fig. 4(a) and 4(b) respectively; time of arrival at each frequency for the hammer (c) and strain (d) signals.

Estimation Procedure using guided waves: To test the effectiveness of the proposed approach the group velocity of the Ao mode propagating in the aluminum plate and shown in Fig.5(b) was used to predict the elastic constants E, G. The identification procedure is based on the minimization of a cost function c that needs to be minimized. The iterative procedure for the identification of the elastic constants is interrupted only when the following convergence criterion is satisfied:

$$c = \sum_{f_i} \left[\frac{C_g^{\exp}(f_i) - C_g^{SAFE}(f_i)}{C_g^{SAFE}(f_i)} \right]^2 < \varepsilon \tag{29}$$

where ε is a predefined tolerance. If Eq.(29) is not verified, the elastic constants E, G (in an isotropic plate) are updated. A MATLAB code was

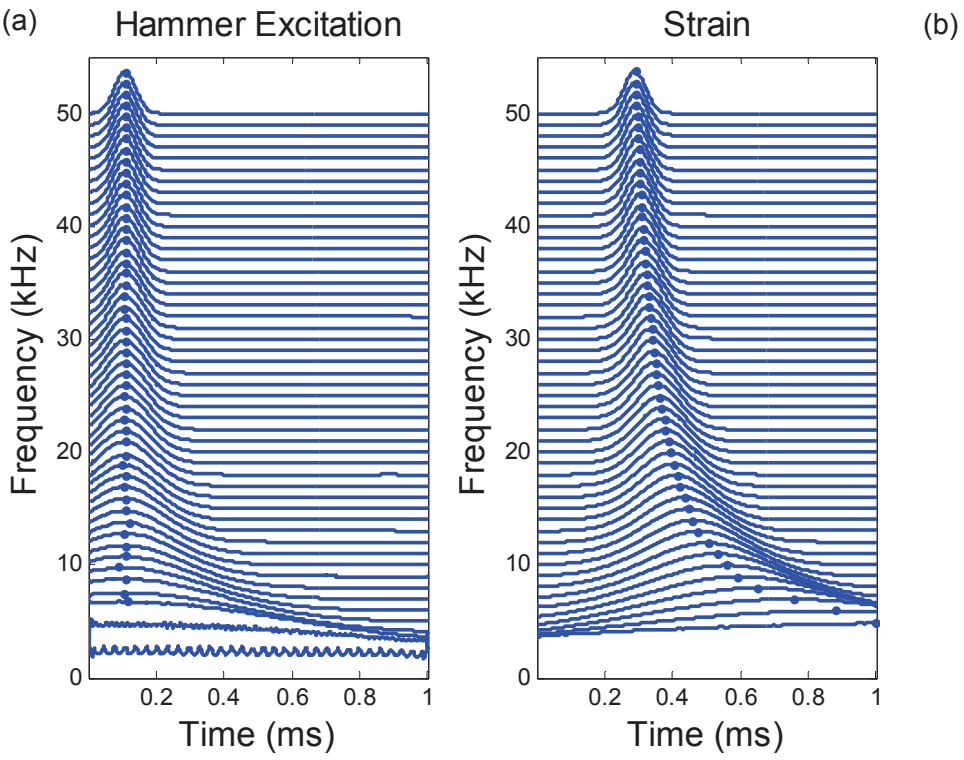

Figure 6: Water fall plot analogous to the Complex Morlet wavelet scalogram for the hammer (a) and strain (b) waveforms.

implemented to update the constants. In the routine, a MATLAB optimization function *fminsearch* updates the unknown parameters used by the SAFE algorithm to compute the updated numerical group velocity $C_g^{SAFE}(f)$. The function *fminsearch* uses the Nelder-Mead simplex algorithm to find minimum of unconstrained multivariable functions using a derivative-free method [18].

The comparison between experimental and numerical group velocity obtained at the end of the identification procedure is shown in Fig.7 while the identification results are summarized in Table 2. It should be noted that while assuming fairly inaccurate initial values of the elastic constants, the final values of E and Gconverge to the same estimates. The same approach was used to estimate the elastic engineering constants of a carbon fiber-reinforced

Table 2: Estimates of the elastic constants for the 3.175 mm thick aluminum plate.

Initial E [GPa]	Initial [GPa]	Predicted E [GPa]	Predicted G [GPa]
120	50	71.04	25.32
115	45	71.04	25.33
110	50	71.06	25.34
105	55	71.02	25.31
100	40	71.02	25.32
95	55	71.04	25.33
90	50	71.06	25.35
85	35	71.03	25.32
80	30	71.06	25.34
75	35	71.04	25.33
70	25	71.03	25.32
65	30	71.05	25.33
65	35	71.03	25.32
60	30	71.01	25.31
55	35	71.07	25.32

plastic (CFRP) laminated composite plate. Total thickness of the plate is 1.6 mm. The plate is square with dimensions of 0.33m×0.33m. Excitation was provided by a pencil lead break (allowing for a frequency range from DC to 200kHz). Since this source does not allow to trigger the event, two sensors were required to compute the wave velocity. Signals were recorded by a Macro fiber composite transducers (MFC) bonded to the surface of the carbon fiber composite plate. Fig.8(a) and (b) show the time waveform and the scalogram for one of the signals acquired. A sensitivity study demonstrated

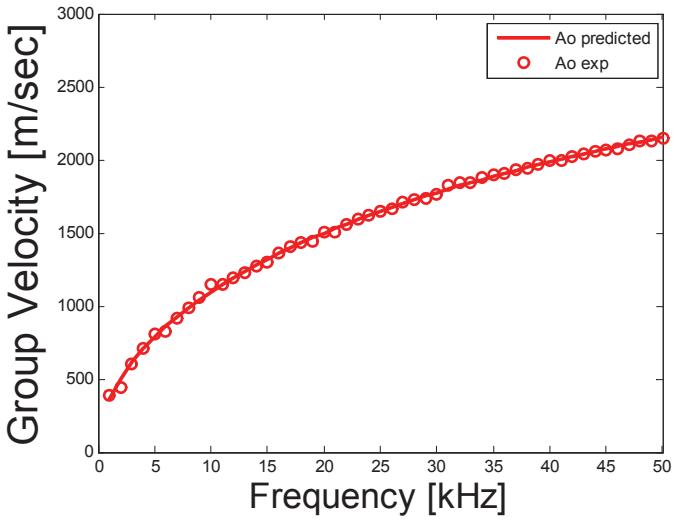

Figure 7: Comparison between experimental (Continuous Wavelet Transform) and numerical (SAFE) group velocities for the Ao mode propagating in a 3.175mm thick aluminum plate.

that the engineering constants that affect the A_0 mode are the Young modulus E_{11}, E_{22} and the shear stiffnesses G_{13} and G_{23}. These four constants were assumed as the independent parameters in the case considered. In fact, the plate that is composed by 12 layers with a staking sequence $[0/\pm 45]_{2S}$, has layers that can be assumed as transversely isotropic laminas. For transversely isotropic layers, five independent constants are generally present but Poisson's ratios influence on wave velocity of the A_0 mode is negligible. To extract Poisson's ratio, the symmetric mode So should be considered as well in the identification approach.

Numerical simulations and signal processing followed the same criteria

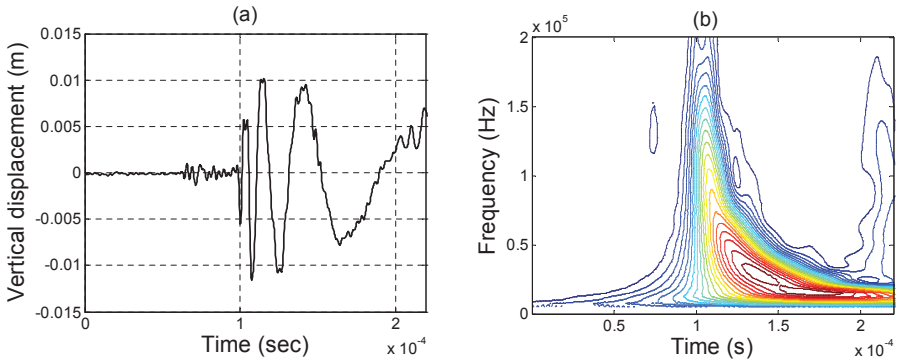

Figure 8: (a) Time history and (b) Complex Morlet wavelet scalogram of waveform generated by a pencil lead break test and recorded by an MFC transducer bonded to a 1.6mm thick carbon fiber-reinforced plastic (CFRP) laminated composite plate.

Table 3: Estimates of the elastic constants for the 1.6 mm thick (CFRP) composite plate.

	Initial values	Predicted values
	[GPa]	[GPa]
E_{11}	85	136.7
G_{13}	5.32	5.08
G_{23}	2.59	3.16

described for the isotropic plate. However, since the frequency range considered for the composite plate was DC-200kHz, a complex Morlet mother wavelet with a central frequency equal to 5 and a bandwidth equal to 2 was used in the CWT. Fig.9 shows the results of the identification approach. A good agreement between the group velocity dispersion curves obtained experimentally and numerically can be observed. Results of the identification procedure are summarized in Table 3.

Although more tests should be performed on a variety of plates to better validate the procedure proposed, the use of guided waves seems ideal to perform the identification of out of plane elastic constants of composite plates. In particular, the potential for the identification of hard to measure constants such as the out of plane shear constants could improve other dynamic

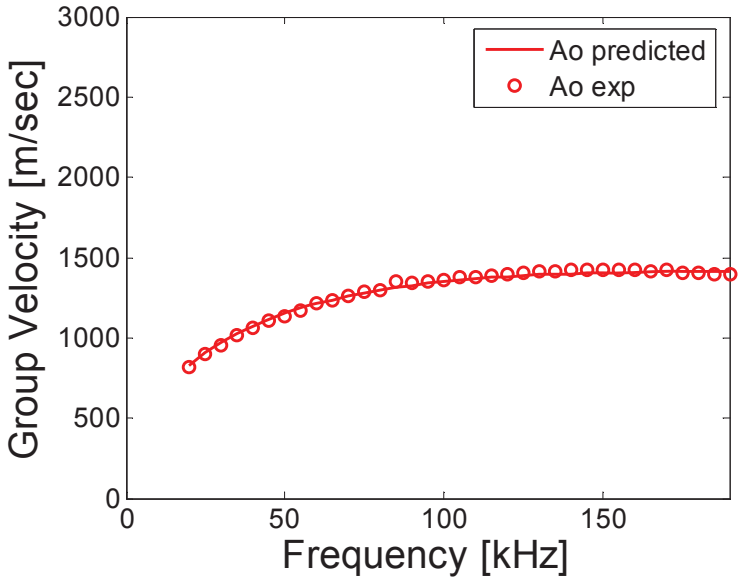

Figure 9: Comparison between experimental and numerically predicted group velocities for the fundamental antisymmetric Ao mode propagating in a 1.6mm thick (CFRP) laminated composite plate.

identification approaches based on the natural frequencies of the plate.

An ideal set-up combining global vibrations and transient guided wave vibrations will not require additional hardware. The excitation for both global (low frequency) vibrations and transient (high frequency) waves could be provided by a small instrumented impact hammer. Vibrations could be measured by accelerometers or alternatively using laser vibrometer. The major factor is represented by the sampling rate at which the waveforms/signals are recorded. While 10000 Hz will be sufficient for the low frequency vibrations, sampling frequencies of 1-5MHz are common when recording guided waves.

4 Conclusions

Two approaches for mechanical parameter identification of composite plates were presented. The techniques use the dynamic properties of the plate. One approach identifies the elastic constants by minimizing the difference between

experimentally measured and numerically predicted natural frequencies related to the global vibrations of the panels. While potentially very robust, this approach cannot reliably predict out of plane shear constants and Poisson's ratio in thin plates because such parameters have little or no effect on the flexural vibrations considered at low frequencies.

A second approach, based on the comparison between experimental and numerically predicted dispersion properties (such as group velocities of guided waves) shows the potential to solve these problems. For example, flexural modes such as the fundamental Ao guided mode can be used to predict out of plane shear constants and axial modes such as the symmetric So mode (not discussed here) could be employed to predict the Poisson's ratio.

The authors believe that a combination of the two approaches above (global/low frequency and transient/high frequency identification techniques) could provide an excellent nondestructive way to reliably estimate all the relevant mechanical properties of composite structural elements.

References

[1] L.R. Deobald and R.F. Gibson, Determination of elastic constants of orthotropic plates by modal analysis/Rayleigh-Ritz technique, J. Sound Vib., 124, (1988), 269–283.

[2] A.L. Araujo, C.M. Mota Soares, M.J. Moreira di Freitas, P. Pedersen, J. Herskovits, Combined numerical-experimental model for the identification of mechanical properties of laminated structures, Compos. Struct. 50, (2000), 363-72.

[3] P.S. Frederiksen, Experimental Procedure and Results for the Identification of Elastic Constants of Thick Orthotropic Plates, J. Compos. Mater., 31, (1997), 360–382.

[4] A.K. Bledzki, A. Kessler, R. Rikards, A. Chate, Determination of elastic constants of glass/epoxy unidirectional laminates by the vibration testing of plates. Compos. Sci. Technol., 59, (1999), 2015-24.

[5] T.C. Lai, K.H. Ip, Parameter estimation of orthotropic plates by Bayesian sensitivity analysis. Compos. Struct., 34 (1996), 29-42.

[6] F. Daghia, S. De Miranda, F. Ubertini, and E. Viola, "Estimation of elastic constants of thick laminated plates within a Bayesian framework," Compos. Struct., 80, (2007), 461–473.

[7] T. Marwala, and S. Sibisi, Finite Element Model Updating Using Bayesian Framework and Modal Properties, Journal of Aircraft, 42, (2005), 275–278.

[8] C. Gogu, R. Haftka, R. Le Riche, J. Molimard, and A. Vautrin, Introduction to the Bayesian approach applied to elastic constants identification, AIAA Journal, 48, (2010), 893-903.

[9] C. Maletta, and L. Pagnotta, On the determination of mechanical properties of composite laminates using genetic algorithms, Int. J. Mech. Mater. Des., 1, (2004), 199–211.

[10] J.N. Reddy, Mechanics of laminated composite plates, CRC Press, New York, 1996.

[11] R.M. Jones, Mechanics of composite materials, Scripta Book Co., Washington, 1975.

[12] J.H. Kim, H.S. Kim, A study on the dynamic stability of plates under a follower force, Computers and Structures, 74, (2000), 351-363.

[13] I. Bartoli, A. Di Leo, E. Viola, Parameter estimation of fiber reinforced composite materials using Bayesian sensitivity analysis. In Proc. Comp. in Constr. Int. Conf., (2003), 595–600.

[14] T. Hayashi, W.J. Song, and J.L. Rose, Guided wave dispersion curves for a bar with an arbitrary cross-section, a rod and rail example, Ultrasonics, 41, (2003), 175-183.

[15] I. Bartoli, A. Marzani, F. Lanza di Scalea, and E. Viola, Modeling Wave Propagation in Damped Waveguides of Arbitrary Cross-section, J. Sound Vib., 295, (2006), 685-707.

[16] K. Kishimoto, H. Inoue, M. Hamada, and T. Shibuya, Time Frequency Analysis of Dispersive Waves by Means of Wavelet Transform, J. Appl. Mech., 62, (1995), 841-846.

[17] S.G. Mallat, A Wavelet tour of signal processing, Academic Press, New York, 1999.

[18] J.C. Lagarias, J.A. Reeds, M.H. Wright, and P.E. Wright, "Convergence Properties of the Nelder-Mead Simplex Method in Low Dimensions." SIAM Journal of Optimization, 9, (1998), 112–147.

Submitted in June 2011

Identifikacija mehaničkih svojstava kompozitnih konstruktivnih elemenata na bazi kombinovanog frekvencionog pristupa

U radu je predložen hibridni postupak kojim se uporedjuju eksperimentalno odredjena dinamička svojstva ploča, kao sto su modalne frekvence i disperzivna svojstva talasa u njima, sa korespondentnim svojstvima koja su odredjena numeričkim postupkom. U semi-analitički model, koji je kombinovan sa metodom konačnih elemenata, ugradjena je numerički efikasna iterativna procedura.

doi:10.2298/TAM1201001B Math.Subj.Class.: insert from AMS classification